UCI-HEP-TR-2021-23, IPPP/21/52

Dark Matter Freeze-out during $\mathrm{SU(2)_L}$ Confinement

Jessica N. Howard,[a] **Seyda Ipek,**[b] **Tim M.P. Tait,**[a] **Jessica Turner**[c]

[a] *Department of Physics and Astronomy, University of California, Irvine, CA 92697 USA*

[b] *Department of Physics, Carleton University, Ottawa, ON, Canada*

[c] *Institute for Particle Physics Phenomenology, Durham University, South Road, Durham, U.K.*

E-mail: jnhoward@uci.edu, sipek@physics.carleton.ca, ttait@uci.edu, jessica.turner@durham.ac.uk

Abstract: We explore the possibility that dark matter is a pair of vector-like fermionic $\mathrm{SU(2)_L}$ doublets and propose a novel mechanism of dark matter production that proceeds through the confinement of the weak sector of the Standard Model. This confinement phase causes the Standard Model doublets and dark matter to confine into pions. The dark pions freeze-out before the weak sector deconfines and generate a relic abundance of dark matter. We solve the Boltzmann equations for this scenario to determine the scale of confinement and constituent dark matter mass required to produce the observed relic density. We determine which regions of this parameter space evade direct detection, collider bounds, and successfully produce the observed relic density of dark matter. For a TeV scale pair of vector-like fermionic $\mathrm{SU(2)_L}$ doublets, we find the weak confinement scale to be ~ 700 TeV.

Contents

1 Introduction

The identity of the dark matter and its role in a theory of fundamental interactions remains one of the most pressing open questions today, and drives a vibrant program of experimental and theoretical research into Physics beyond the Standard Model (SM) [1]. A key property that distinguishes among different possibilities is the nature of the interactions between the dark matter and the ingredients of the Standard Model, typically characterized by the masses and couplings of the mediator particles.

An economical choice is to allow the dark matter to transform under the SM's $SU(2)_L$ weak interaction, repurposing the electroweak bosons of the Standard Model (W, Z, and h) as the mediators. This results in a prototypical weakly interacting massive particle (WIMP), whose abundance in the Universe can be naturally understood as a result of it freezing out after an initial period of chemical equilibrium with the SM plasma [2]. While attractive, an $SU(2)_L$-charged WIMP whose abundance is set by freeze-out is highly constrained. The TeV masses favored by the dark matter abundance often predict signals which are expected to have been visible at colliders [3, 4], in searches for ambient dark matter scattering with heavy nuclei [5], and by searches for high energy annihilation products which make their way to the Earth [6]. With dominant couplings typically fixed by $SU(2)_L$ gauge invariance, a specific choice

of $SU(2)_L$-charged WIMP freezes out with the correct abundance for only a very narrow range of masses. While windows of viable parameter space exist (see e.g. Ref. [7]), many types of $SU(2)_L$-charged WIMPs naively appear to be excluded as relics whose abundance is determined by freeze-out.

An $SU(2)_L$-charged WIMP typically freezes out at a temperature $\simeq M/20$, which for an electroweak-sized mass corresponds to a period of cosmology that is much earlier than Big Bang Nucleosynthesis, and thus during an epoch that is relatively unconstrained by observational data. At this time, the Universe may deviate dramatically from our extrapolation based on the SM, due to unforeseen Physics beyond the Standard Model. Indeed, explorations of non-standard cosmological histories, including a period of early matter domination [8], late entropy injection [9], and modifications of fundamental parameters such as the strength of the SU(3) coupling [10, 11] have all been shown to lead to dramatically different expectations in the mapping of WIMP parameter space onto its predicted abundance in the early Universe.

This article explores a non-standard cosmology that can dramatically change the favored mass range for an $SU(2)_L$-charged WIMP, which makes up the bulk of the dark matter. We introduce dynamics that modify the value of the $SU(2)_L$ interaction strength very early, causing it to confine [12]. This weak confinement causes the left-chiral quarks and leptons of the SM, and a new vector-like pair of fermionic doublets that plays the role of dark matter, to bind into composite pion-like states that are $SU(2)_L$ neutral. The freeze-out process involves those pions containing the dark matter annihilating into lighter pions composed entirely of SM fermions. At some time after freeze-out, the $SU(2)_L$ interaction returns to its currently observed value, at which point the pions deconfine, leaving behind the frozen out dark matter. A sketch of this cosmological history is shown in Fig. 1.

Our work is organized as follows: in Section 2, we introduce the description of the Universe during an early period of $SU(2)_L$ confinement, including an additional vector-like pair of fermionic doublets which can play the role of dark matter. In Section 3 we discuss the freeze-out process in detail and identify the parameter space leading to the observed abundance of dark matter today and our results are summarized in Fig. 4. The more realistic case including three generations of SM fermions is discussed in Section 4. Finally, we conclude in Section 5 and provide technical details in the appendices.

2 Weak Confinement and Dark Matter

Our dark matter production mechanism involves a temporary cosmological era of $SU(2)_L$ confinement. The possibility that the weak sector was strong in the early universe was initially proposed in [13–16] (see also [17–20]) and the cosmological consequences of such a scenario were studied in Ref. [12]. We refrain from rederiving the complete results of Ref. [12], which gives a detailed discussion of the gauge and global symmetry breaking patterns as well as the particle content of the confined phase, and instead highlight some key results pertinent for this work:

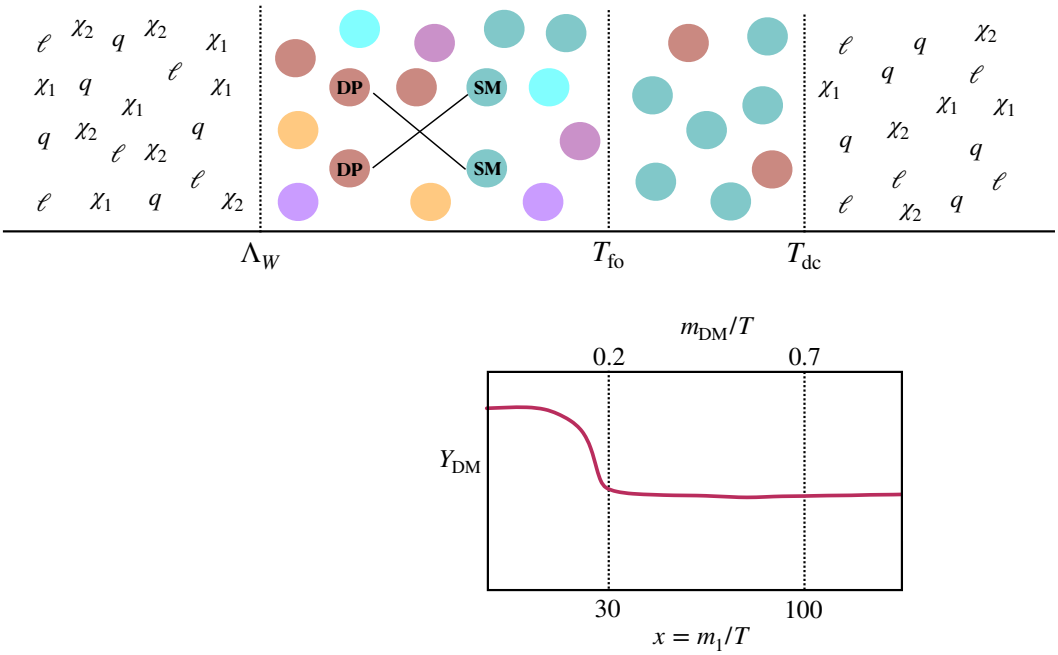

Figure 1: Upper panel: A sketch of the cosmological history of the Universe where we assume a period of weak confinement begins at Λ_W, at which point the DM (χ_1, χ_2) and SM (q, ℓ) doublets are bound into weak pions. During this epoch, the freeze-out of dark pions takes place at $T_{\rm fo}$, followed by deconfinement at $T_{\rm dc}$. Lower panel: The evolution of the dark pion abundance for a representative value of the freeze-out temperature $x_{\rm fo} = m_1/T_{\rm fo} \simeq 30$, corresponding to a temperature of $0.2 m_{\rm DM}$. In our notation, m_1 and $m_{\rm DM}$ denote the lightest dark pion and the constituent dark matter masses respectively, see Section 3 for details.

- Weak confinement causes the $\mathrm{SU}(2)_{\rm L}$ doublets to condense into bound states analogous to the mesons and baryons of QCD. The lowest-lying states are mesons, Π and η', composed of the SM lepton and quark doublets, l and q respectively. These states are contained in the complex antisymmetric scalar field, Σ_{ij}, where $i, j = 1, ..., 2N_f$ with $2N_f$ of left-chiral Weyl fermion fields. For the Standard Model with three generations, $N_f = 6$.

- Following intuition based on chiral symmetry breaking in QCD [21, 22] and evidence from lattice simulations, there is a chiral condensate spontaneously breaking the global symmetry: $\mathrm{SU}(2N_f) \to \mathrm{Sp}(2N_f)$ [23–29]. This pattern of symmetry breaking is encoded by the antisymmetric field Σ_{ij} acquiring a vacuum expectation value $\langle \Sigma_{ij} \rangle = (\Sigma_0)_{ij}$ that satisfies $\Sigma_0^\dagger \Sigma_0 = \Sigma_0 \Sigma_0^\dagger = \mathbb{1}$. Neglecting the other SM gauge interactions and Yukawas, this symmetry breaking results in $2N_f^2 - N_f - 1$ massless Goldstone bosons (GBs) and a single massive pseudo-Goldstone boson (PGB), analogous to the η' of QCD.

- The dynamics of the confined theory are described by an infrared Lagrangian which is

constructed from the scalar field Σ_{ij} that contains the massive PGB and massless GBs:

$$\Sigma = \exp\left[i\eta'/\sqrt{N_f}f\right] \exp\left[\sum_a 2iX^a\Pi^a/f\right] \Sigma_0 \,, \tag{2.1}$$

where X^a_{ij} are the $2N_f^2-N_f-1$ broken generators of $\mathrm{Sp}(2N_f)$ and f is the decay constant. Considering the three SM generations of $\mathrm{SU(2)_L}$ doublets, there are 65 massless pions. However, loop-induced corrections from the SM gauge and Yukawa interactions provide masses to 58 of the 65 pions.

- Weak confinement breaks the gauge symmetry of the Standard Model from $\mathrm{SU(3)_C} \times \mathrm{U(1)_Y}$ to $\mathrm{SU(2)_C} \times \mathrm{U(1)_Q}$, resulting in four massless gauge bosons ($G^{1,2,3}, A'$) and five massive gauge bosons, which can be arranged into a pair of complex gauge bosons ($W'^{\pm}$) and single real vector boson (Z').

We augment the SM particle content by two $\mathrm{SU(2)_L}$ doublets, χ_1 and χ_2 (of hypercharges $\pm 1/2$, respectively), which play the role of dark matter. They are assembled into a pseudo-Dirac state,

$$\mathcal{L}_\chi = i\chi_1^\dagger \bar{\sigma}^\mu D_\mu \chi_1 + i\chi_2^\dagger \bar{\sigma}^\mu D_\mu \chi_2 + m_{\mathrm{DM}}\ \chi_1\chi_2 + \mathrm{h.c}\,, \tag{2.2}$$

where D_μ is a covariant derivative of the unconfined phase and m_{DM} is the mass of the constituent dark matter. This Lagrangian is invariant under a $\mathrm{U(1)}_\chi$ symmetry under which χ_1 (χ_2) are charged ± 1 that ensures their stability.

The infrared Lagrangian, describing the dynamics of the confined theory, has the form

$$\mathcal{L}_{\mathrm{IR}} \supset \frac{f^2}{4}\,\mathrm{Tr}\left[D_\mu\Sigma^\dagger D^\mu\Sigma\right] + \Lambda_W^3\,\mathrm{Tr}[M\Sigma + \Sigma^\dagger M^T] + \kappa\Lambda_{\mathrm{W}}^2 f^2 \mathrm{Re}[\det\Sigma] + \Delta\mathcal{L}\,, \tag{2.3}$$

where D_μ is a covariant derivative of the confined phase, $\Lambda_{\mathrm{W}} \sim 4\pi f$ is the weak confinement scale, κ is an $\mathcal{O}(1)$ dimensionless number, and M is the mass matrix, treated as an $\mathrm{SU}(2N_f)$-breaking spurion in the limit $m_{\mathrm{DM}} \ll \Lambda_{\mathrm{W}}$. In the simplified case where we consider a single generation of $\mathrm{SU(2)_L}$ doublets together with the dark matter, $2N_f = 6$ and the mass matrix, defined in the basis $\{\ell, q^R, q^G, q^B, \chi_1, \chi_2\}$ where R, G, and B denote the colors of $\mathrm{SU(3)_C}$, is:

$$M = \frac{m_{\mathrm{DM}}}{2}\begin{pmatrix} 0 & 0 & 0 & 0 & 0 & 0 \\ 0 & 0 & 0 & 0 & 0 & 0 \\ 0 & 0 & 0 & 0 & 0 & 0 \\ 0 & 0 & 0 & 0 & 0 & 0 \\ 0 & 0 & 0 & 0 & 0 & 1 \\ 0 & 0 & 0 & 0 & -1 & 0 \end{pmatrix}. \tag{2.4}$$

The infrared Lagrangian also contains operators reflecting the explicit breaking of $SU(2N_f)$ by the gauging of $SU(3)_C$ and $U(1)_Y$:

$$\begin{aligned}\Delta\mathcal{L} = C_G\Lambda_W^2 f^2 \frac{g_s^2}{16\pi^2}\sum_{a=1,2,3}\mathrm{Tr}[L^a\Sigma^\dagger L^{aT}\Sigma] + C_A\Lambda_W^2 f^2\frac{e_Q^2}{16\pi^2}\mathrm{Tr}[Q\Sigma^\dagger Q\Sigma] \\ + C_W\Lambda_W^2 f^2\frac{g_s^2/2}{16\pi^2}\sum_{\pm}\sum_{i=1,2}\mathrm{Tr}[L^{i\pm}\Sigma^\dagger L^{i\pm}\Sigma] + C_Z\Lambda_W^2 f^2\frac{e_Q^2/s_Q^2c_Q^2}{16\pi^2}\ \mathrm{Tr}[J\Sigma^\dagger J\Sigma]\,,\end{aligned} \tag{2.5}$$

where the dimensionless coefficients, C_G, C_A, C_W, and C_Z, encode the non-perturbative $SU(2)_L$ dynamics, and are expected to be $\mathcal{O}(1)$ [30, 31]. The $SU(2)_C$ and hypercharge couplings are denoted as g_s and g', respectively, and $\sin\theta_Q = g'/\sqrt{3g_s^2+g'^2}$ with $e_Q \approx g'$ in the limit, $g' \ll g_s$. The generators of the $SU(2)_C$ and $U(1)_Q$ are denoted as L^a and Q, respectively, and $L^\pm$ is a combination of $SU(3)_C$ generators which couple to the massive vector fields $W'^\pm$. Finally, J is a combination of an $SU(3)_C$ and an $U(1)_Q$ generator which couple to the massive Z' gauge boson (see Appendix A and Ref. [12] for further details).

For the remainder of this Section, we consider a simplified toy model consisting of one SM generation of fermionic doublets together with χ_1 and χ_2 (corresponding to $N_f = 3$, for which there are 14 broken generators of the SU(6) flavor symmetry). This allows us to extract the most important points in a framework that is simpler to analyze. We return to the more realistic case of three generations plus $\chi_{1,2}$ (corresponding to $N_f = 14$) in Section 4.

2.1 Pion Masses and Mass Eigenstates

The mass spectrum of the pions during weak confinement is determined from the terms of Eq. (2.3) that are quadratic in the meson fields, $\mathcal{L}_{IR} \to -(1/2)(M_\Pi^2)_{ab}\Pi^a\Pi^b$. Following Ref. [12], we define M_Π^2 in the basis $\Pi = \{\eta', \Pi^a\}$ where $a = 1...14$. In contrast to the case studied in [12], the resulting mass matrix contains non-diagonal entries mixing the η' with the meson dominantly composed of $\chi_1\chi_2$:

$$M_\Pi^2 = \begin{pmatrix} M_{0,0}^2 & . & . & . & M_{0,14}^2 \\ . & M_{1,1}^2 & . & . & . \\ . & . & . & . & . \\ . & . & . & M_{13,13}^2 & . \\ M_{0,14}^2 & . & . & . & M_{14,14}^2 \end{pmatrix}, \tag{2.6}$$

and thus the interaction and mass eigenstates are not aligned. We rotate to the mass basis via the unitary transformation $\Pi \to W\Pi$, for which

$$M_{\mathrm{diag}}^2 = W M_\Pi^2 W^{-1}\,, \tag{2.7}$$

where W is a unitary matrix

$$W = \begin{pmatrix} \cos\theta & . & . & . & \sin\theta \\ . & 1 & . & . & . \\ . & . & . & . & . \\ . & . & . & 1 & . \\ -\sin\theta & . & . & . & \cos\theta \end{pmatrix} , \tag{2.8}$$

with

$$\tan 2\theta = 2\frac{M_{0,14}^2}{(M_{0,0}^2 - M_{14,14}^2)} , \tag{2.9}$$

and

$$M_{0,0}^2 = 24\kappa\Lambda_W^2 + \frac{2\Lambda_W^3 m_{\rm DM}}{3f^2} , \quad M_{0,14}^2 = -\frac{2\sqrt{2}\Lambda_W^3 m_{\rm DM}}{3f^2} , \quad M_{14,14}^2 = \frac{4\Lambda_W^3 m_{\rm DM}}{3f^2} . \tag{2.10}$$

Substituting Eq. (2.10) into Eq. (2.9), we find that

$$\tan 2\theta = \frac{2\sqrt{2}\pi m_{\rm DM}}{\pi m_{\rm DM} - 9\kappa f} \approx -\frac{2\sqrt{2}\pi m_{\rm DM}}{9\kappa f} + \mathcal{O}\left(\frac{m_{\rm DM}^2}{f^2}\right) , \tag{2.11}$$

where we have taken $\Lambda_W = 4\pi f$. Throughout we assume that $m_{\rm DM} \ll f$ and this implies that the mixing between η' (which we label as Π_0) and the $\chi_1\chi_2$ (which we label as Π_{14}) state is small, $\cos\theta \approx 1$ and $\sin\theta \approx \theta$, and this leads to:

$$\Pi_0^{\rm mass} \approx \Pi_0^{\rm int} + \theta\Pi_{14}^{\rm int} , \tag{2.12a}$$

$$\Pi_{14}^{\rm mass} \approx \Pi_{14}^{\rm int} - \theta\Pi_0^{\rm int} , \tag{2.12b}$$

where $\Pi_i^{\rm mass} = \Pi_i^{\rm int}$ for $i = 1, ..., 13$. The masses of $\Pi_0^{\rm mass}$ and $\Pi_{14}^{\rm mass}$ are:

$$\begin{aligned} M_0^2 &\approx 384\pi^2 f^2 \kappa \left(1 + \frac{\pi m_{\rm DM}}{9\kappa f} + \mathcal{O}\left(\frac{m_{\rm DM}^2}{f^2}\right)\right) , \\ M_{14}^2 &\approx \frac{256\pi^3}{3} f m_{\rm DM} \left(1 - \frac{\pi m_{\rm DM}}{9\kappa f} + \mathcal{O}\left(\frac{m_{\rm DM}^2}{f^2}\right)\right) . \end{aligned} \tag{2.13}$$

Table 1 shows the approximate masses of the 15 mesons for the one generation SM case, as well as their representations under the residual $\mathrm{U}(1)_{\rm Q} \times \mathrm{SU}(2)_{\rm C}$ gauge symmetries, in the small mixing limit.

The specific pion masses depend on the non-perturbative coefficients C_G, C_A, C_Z, C_W, and κ. These could in principle be determined from lattice simulations, and are expected to be $\mathcal{O}(1)$ based on arguments from naive dimensional analysis [32]. We proceed under the assumption that $C_G = C_A = C_Z = -1$ and $C_W = \kappa = 1$. As is evident from Table 1, the masses of $\Pi_{1,2,3,4}^{\rm mass}$ are independent of $m_{\rm DM}$, reflecting the fact that they are purely composed of SM quark and lepton doublets, with masses generated via SM gauge interactions, Eq. (2.5), and are typically the lightest of the massive pions. The $\Pi_0^{\rm mass}$ is significantly heavier than

Pion	Mass^2	$\mathrm{U(1)_Q}$	$\mathrm{SU(2)_C}$	content
$\Pi_0^{\rm mass}$	$384\pi^2 f^2\kappa$	0	1	χ_1, χ_2
$\Pi_{1,2,3,4}^{\rm mass}$	$-\frac{1}{2}C_A e_Q^2 f^2 - \frac{3}{2}C_G f^2 g_s^2 + C_W f^2 g_s^2 + \frac{C_Z e_Q^2 f^2}{6 s_Q^2} + \frac{1}{2}C_Z e_Q^2 f^2$	±1	2	ℓ, q_D, q_S
$\Pi_{5,8}^{\rm mass}$	$64\pi^3 f m_{\rm DM}$	0	1	χ_1, χ_2, q_S
$\Pi_{6,7}^{\rm mass}$	$-2C_A e_Q^2 f^2 - 2C_Z e_Q^2 f^2 s_Q^2 + \frac{2}{3}C_Z e_Q^2 f^2 + 64\pi^3 f m_{\rm DM}$	±1	1	$\ell, \chi_1, \chi_2, q_S$
$\Pi_{9,10,11,12}^{\rm mass}$	$-\frac{1}{2}C_A e_Q^2 f^2 - \frac{3}{2}C_G f^2 g_s^2 + \frac{C_Z e_Q^2 f^2}{18 s_Q^2} + 64\pi^3 f m_{\rm DM}$	±1	2	χ_1, χ_2, q_D
$\Pi_{13}^{\rm mass}$	0	0	1	ℓ, q_S
$\Pi_{14}^{\rm mass}$	$\frac{256}{3}\pi^3 f m_{\rm DM}$	0	1	χ_1, χ_2

Table 1: Masses of the pions (for the one SM generation case) in the small mixing limit, along with their $\mathrm{U(1)_Q}\times\mathrm{SU(2)_C}$ charges and constituent $\mathrm{SU(2)_L}$ doublet content.

the other mesons, rendering it unimportant for the freeze-out dynamics due to Boltzmann suppression. We observe that $\Pi_{14}^{\rm mass}$ is 4/3 times heavier than $\Pi_{5,8}^{\rm mass}$ and hence, we can ignore the effect of $\Pi_{14}^{\rm mass}$ in calculating the dark matter dynamics. In Fig. 2, we show the pion masses as a function of $m_{\rm DM}$ for $f = 65$ TeV, corresponding to $\Lambda_W \approx 800$ TeV (this choice is motivated by discussions of DM abundance in Section 3). We examine two benchmark cases: BP1 where g_s, g' and $s_Q = g'/\sqrt{3g_s^2 + g'^2}$ are found by evaluating the running SM coupling constants to approximately Λ_W and BP2, which is similar to a regime of interest from Ref. [12]. More specifically:

$$\begin{aligned} &\text{BP1} \quad g_s = 0.8\,, \quad e_Q = 0.5\,, \quad s_Q^2 = 0.12\,, \\ &\text{BP2} \quad g_s = 0.1\,, \quad e_Q = 0.01\,, \quad s_Q^2 = 3.3\times10^{-3}\,. \end{aligned}$$

Fig. 2 indicates that $M_{5,8}, M_{6,7}$ and $M_{9,10,11,12}$ differ slightly due to the loop contributions, and that $M_{5,8}$ are the lightest massive states. BP2 has values of g_s, e_Q which are smaller than those in BP1, leading to much smaller differences between $M_{5,8}, M_{6,7}$ and $M_{9,10,11,12}$, resulting in a more compressed spectrum.

2.2 $\mathrm{U(1)_\chi}$ Eigenstates

$\mathrm{U(1)_\chi}$ remains unbroken during the confined phase, and it is convenient to organize the pions based on their $\mathrm{U(1)_\chi}$ charges. This is evident from the fact that the $\mathrm{U(1)_\chi}$ generator,

$$Q_\chi = \begin{pmatrix} 0 & 0 & 0 & 0 & 0 & 0 \\ 0 & 0 & 0 & 0 & 0 & 0 \\ 0 & 0 & 0 & 0 & 0 & 0 \\ 0 & 0 & 0 & 0 & 0 & 0 \\ 0 & 0 & 0 & 0 & 1 & 0 \\ 0 & 0 & 0 & 0 & 0 & -1 \end{pmatrix}, \tag{2.14}$$

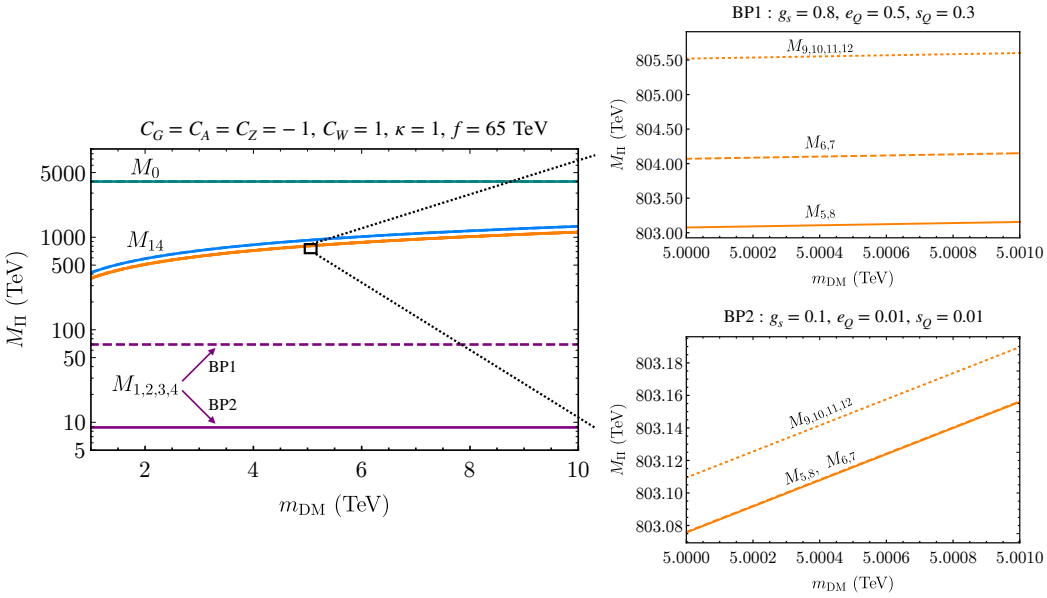

Figure 2: Pion masses as a function of $m_{\rm DM}$, assuming $C_G = C_A = C_Z = -1$, $C_W = 1$ and $\kappa = 1$, for two benchmark points: BP1 where g_s, $e_Q \simeq g'$ and $s_Q \simeq g'/\sqrt{3g_s^2 + g'^2}$ are found by running g_s and g' to $\Lambda_W = 4\pi f \simeq 800$ TeV; and BP2 where we take $g_s = 0.1$ and $e_Q = 0.01$. $M_{13} = 0$ is not shown.

leaves the vacuum invariant: $Q_\chi \Sigma_0 + \Sigma_0 Q_\chi = 0$. To infer the $\mathrm{U}(1)_\chi$ charges of the pions, we transform Σ by an infinitesimal $\mathrm{U}(1)_\chi$ rotation:

$$\Sigma \xrightarrow{\mathrm{U}(1)_\chi} e^{iQ_\chi\theta_\chi}\Sigma(e^{iQ_\chi\theta_\chi})^T \approx \Sigma + i\theta_\chi\left(Q_\chi\Sigma + \Sigma Q_\chi\right) + \dots\,, \tag{2.15}$$

and expand Σ to first order, $\Sigma \simeq \Sigma_0 + \frac{i}{f}\Pi_a X_a \Sigma_0 + ...$, from which we can extract the transformation of each pion:

$$\Pi_b \xrightarrow{\mathrm{U}(1)_\chi} \Pi_b + i\theta_\chi \underbrace{2\Pi_a \mathrm{Tr}[[Q_\chi, X_a], X_b]}_{\delta\Pi_b}\,. \tag{2.16}$$

Using the specific form of the generators X_a and Q_χ we can explicitly evaluate $\delta\Pi_a$ for each $a = 0, ...14$, and construct complex linear combinations of pions fields that have definite $\mathrm{U}(1)_\chi$ charge:

$$\begin{aligned}
\tilde{\Pi}_1^\pm &\equiv \frac{1}{\sqrt{2}}\left(\Pi_5^{\rm mass} \mp i\Pi_8^{\rm mass}\right),\\
\tilde{\Pi}_2^\pm &\equiv \frac{1}{\sqrt{2}}\left(\Pi_6^{\rm mass} \mp i\Pi_7^{\rm mass}\right),\\
\tilde{\Pi}_3^\pm &\equiv \frac{1}{\sqrt{2}}\left(\Pi_9^{\rm mass} \mp i\Pi_{12}^{\rm mass}\right),\\
\tilde{\Pi}_4^\pm &\equiv \frac{1}{\sqrt{2}}\left(\Pi_{10}^{\rm mass} \mp i\Pi_{11}^{\rm mass}\right),
\end{aligned} \tag{2.17}$$

and $\tilde{\Pi}_i^0 \equiv \Pi_i^{\rm mass}$ for $i \in \{0,1,2,3,4,13,14\}$ are left as zero-charge real scalar fields. Note that these redefinitions commute with the mass basis, as expected.

2.3 Pion Interactions

The most important interactions of the pions, for our purposes, are four-point vertices arising as residual strong interactions from the confined $\mathrm{SU}(2)_{\rm L}$ force. These are encoded in the infrared Lagrangian as higher order terms (in powers of Π/f). Expanding Σ to second order:

$$\begin{aligned}\Sigma(x) &= \exp\left[\frac{i\eta'}{\sqrt{N_f}f}\right]\exp\left[i\frac{2\Pi_a(x)X_a}{f}\right]\Sigma_0 \\ &\approx \left[1 + i\left(\frac{2\Pi_a(x)X_a}{f}\right) - \frac{1}{2}\left(\frac{2\Pi_a(x)X_a}{f}\right)^2 + \mathcal{O}\left(\frac{\Pi^3}{3!f^3}\right)\right]\Sigma_0\,,\end{aligned} \tag{2.18}$$

where the relevant terms from Eq. (2.3) take the form:

$$\mathcal{L}_4 = \frac{4}{f^2}\mathrm{Tr}_1(a,b,c,d)\;\Pi_a\Pi_b\partial^\mu\Pi_c\partial_\mu\Pi_d + \frac{2m_{\rm DM}\Lambda_W^3}{3f^4}\mathrm{Tr}_2(a,b,c,d)\;\Pi_a\Pi_b\Pi_c\Pi_d\,, \tag{2.19}$$

with flavor tensors Tr_1 and Tr_2 defined by

$$\begin{aligned}\mathrm{Tr}_1(a,b,c,d) &\equiv \frac{1}{4}\Big(\mathrm{Tr}\left[X_cX_aX_dX_b\right] + \mathrm{Tr}\left[X_aX_cX_dX_b\right]\Big) \\ &\quad - \frac{1}{12}\Big(\mathrm{Tr}\left[X_cX_aX_bX_d\right] + \mathrm{Tr}\left[X_aX_cX_bX_d\right]\Big) - \frac{1}{3}\mathrm{Tr}\left[X_aX_bX_cX_d\right]\,, \\ \mathrm{Tr}_2(a,b,c,d) &\equiv -\mathrm{Tr}\left[AX_aX_bX_cX_d\right]\,,\end{aligned} \tag{2.20}$$

where $A \equiv \mathrm{diag}(\mathbb{0}_{2x2},...,\mathbb{0}_{2x2},\mathbb{1}_{2\times2})$. These expressions are written in the mass basis, and can be transformed into states of definite $\mathrm{U}(1)_\chi$ charge via Eq. (2.17).

Thepions charged under $\mathrm{SU}(2)_{\rm C}$ and $\mathrm{U}(1)_{\rm Q}$ will also have gauge interactions with those gauge bosons, contained in the kinetic terms of Eq. (2.3). However, we have verified that these couplings are small enough at the scales of interest (leading to cross-sections of $\mathcal{O}(10^{-3})$ smaller than those characterizing annihilation into SM pions) that they can be neglected in our freeze-out analysis.

3 Dark Matter freeze-out

At the time of freeze-out, the dark matter particles are bound into *dark pion* (DP) states, and the final abundances of $\chi_{1,2}$ are determined by the frozen-out densities of $\tilde{\Pi}^\pm_{1,2,3,4}$ (each of which contains one χ) and $\tilde{\Pi}^0_0$ and $\tilde{\Pi}^0_{14}$ (each of which contains two χs). In practice, because of the large mass hierarchy between $\tilde{\Pi}^0_{0,14}$ and $\tilde{\Pi}^\pm_{1,2,3,4}$, it is sufficient to neglect the contributions from the two neutral states and to focus on the $\mathrm{U}(1)_\chi$-charged ones.

The relic abundance of the $\tilde{\Pi}_i^\pm$ is controlled by the temperature, $T_{\rm fo}$, at which their number-changing interactions freeze-out from thermal equilibrium, which in turn depends

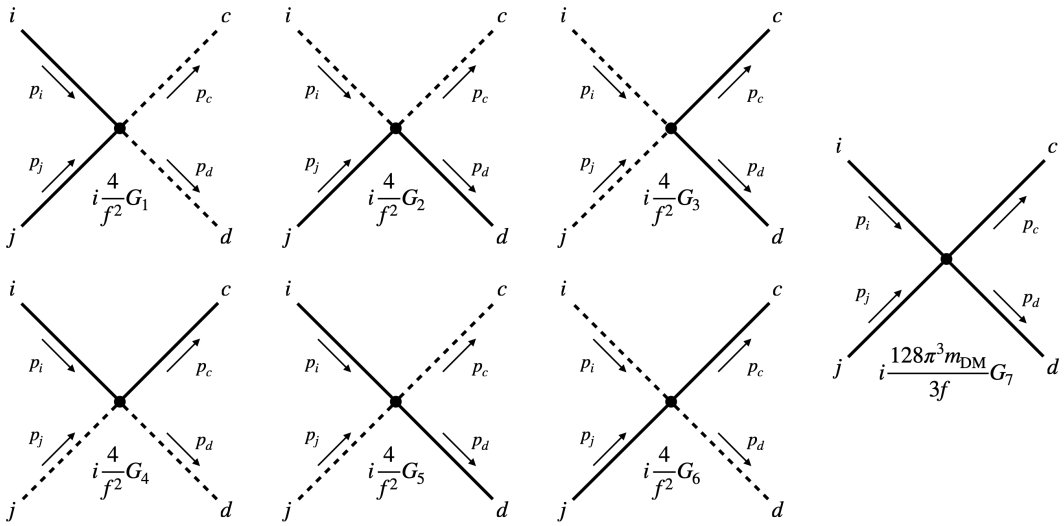

Figure 3: Four-point pion interaction diagrams contributing to the process $\Pi_a\Pi_b \to \Pi_c\Pi_d$. The dashed lines denote fields on which derivatives act, contributing a factor of the corresponding momentum. An incoming (outgoing) field contributes a negative (positive) momentum factor to the matrix element.

sensitively on their annihilation cross sections into the lightest neutral pions comprised of SM doublets: $\tilde{\Pi}_i^+\tilde{\Pi}_j^- \to \tilde{\Pi}_{13}^0\tilde{\Pi}_{13}^0$. The charged states are typically sufficiently close in mass ($\Delta m/T_{\rm fo} \sim 10^{-2}$) that coannihilation processes can be important [33, 34], and are included in our calculations. Nonetheless, the relic abundance is dominated by the annihilation of the lightest DP state into the zero-mass SM pion: $\tilde{\Pi}_1^+\tilde{\Pi}_1^- \to \tilde{\Pi}_{13}^0\tilde{\Pi}_{13}^0$.

3.1 Annihilation Cross-Section

The rate for $\Pi_i\Pi_j \to \Pi_c\Pi_d$ is determined by the Feynman diagrams shown in Fig. 3, where the dashed (solid) lines indicate legs on which derivatives do (do not) act in the corresponding operator. We define the incoming legs to correspond to the pion flavors i, j, and outgoing to c, d. The resulting matrix element, $\mathcal{M}$, takes the form

$$\begin{aligned} i\mathcal{M} = &-i\frac{4(p_c\cdot p_d)}{f^2}G_1 + i\frac{4(p_i\cdot p_c)}{f^2}G_2 - i\frac{4(p_i\cdot p_j)}{f^2}G_3 + i\frac{4(p_j\cdot p_d)}{f^2}G_4 \\ &+ i\frac{4(p_j\cdot p_c)}{f^2}G_5 + i\frac{4(p_i\cdot p_d)}{f^2}G_6 + i\frac{128\pi^3 m_{\rm DM}}{3f}G_7\,, \end{aligned} \tag{3.1}$$

where we used $\Lambda_W = 4\pi f$ and define:

$$\begin{aligned} &G_1 = {\rm Tr}_1(i,j,c,d)\,, \quad G_2 = {\rm Tr}_1(d,j,c,i)\,, \quad G_3 = {\rm Tr}_1(c,d,i,j)\,, \quad G_4 = {\rm Tr}_1(i,c,j,d)\,, \\ &G_5 = {\rm Tr}_1(i,d,c,j)\,, \quad G_6 = {\rm Tr}_1(c,j,i,d)\,, \quad G_7 = {\rm Tr}_2(i,j,c,d)\,, \end{aligned}$$

where Tr_1 and Tr_2 are given in Eq. (2.20). Subsequently, the annihilation cross-section can be expressed as,

$$\sigma_{ij}(s) = \frac{1}{16\pi}\frac{1}{\lambda(s,m_i^2,m_j^2)}\left[C_{\rm const}(t_+ - t_-) + \frac{1}{2}C_{\rm lin}(t_+^2 - t_-^2) + \frac{1}{3}C_{\rm quad}(t_+^3 - t_-^3)\right], \quad (3.2)$$

where λ is the well-known Källén function, $\lambda(x,y,z) \equiv (x-y-z)^2 - 4yz$, and

$$\begin{aligned} t_+ &= m_c^2 + m_i^2 - 2E_cE_i + 2|\vec{p}_c||\vec{p}_i|\,, \\ t_- &= m_c^2 + m_i^2 - 2E_cE_i - 2|\vec{p}_c||\vec{p}_i|\,. \end{aligned} \quad (3.3)$$

The above traces define the coefficients inside the square brackets as:

$$\begin{aligned} C_{\rm const} &\equiv \left(\frac{128\pi^3 m_{\rm DM}}{3f}\right)^2 |C|^2 + \frac{4s^2}{f^4}|G_{13,56}|^2 - \frac{2s}{f^2}\left(\frac{128\pi^3 m_{\rm DM}}{3f}\right)\left[C^* G_{13,56} + C G^*_{13,56}\right], \\ C_{\rm lin} &\equiv \frac{4s}{f^4}\left(G_{13,56}G^*_{24,56} + G^*_{13,56}G_{24,56}\right) - \frac{2}{f^2}\left(\frac{128\pi^3 m_{\rm DM}}{3f}\right)\left[C^* G_{24,56} + C G^*_{24,56}\right], \\ C_{\rm quad} &\equiv \frac{4}{f^4}|G_{24,56}|^2\,, \end{aligned} \quad (3.4)$$

with

$$\begin{aligned} C \equiv G_7 &+ \frac{3m_i^2}{64\pi^3 f m_{\rm DM}}(G_2 + G_3 - G_5) + \frac{3m_j^2}{64\pi^3 f m_{\rm DM}}(G_3 + G_4 - G_6) \\ &+ \frac{3m_c^2}{64\pi^3 f m_{\rm DM}}(G_1 + G_2 - G_6) + \frac{3m_d^2}{64\pi^3 f m_{\rm DM}}(G_1 + G_4 - G_5)\,, \end{aligned} \quad (3.5)$$

$$\begin{aligned} G_{13,56} &\equiv G_1 + G_3 - G_5 - G_6\,, \\ G_{24,56} &\equiv G_2 + G_4 - G_5 - G_6\,. \end{aligned}$$

Note that $64\pi^3 f m_{\rm DM}$ is the mass squared of the lightest pion with DM constituent. In the non-relativistic limit, the $2 \to 2$ scattering cross-section can be expanded in terms of the relative velocity, $v = |\vec{v}_i - \vec{v}_j|$, of the incoming particles,

$$\langle \sigma v \rangle = \sigma_0 + \sigma_2 \langle v^2 \rangle + .. \quad (3.6)$$

At freeze-out, the leading (s-wave) term of this expansion dominates over the order higher terms and hence the velocity averaged cross-section is:

$$\langle \sigma_{ij} v \rangle_{\rm s-wave} = \frac{\lambda^{1/2}(s,m_c^2,m_d^2)}{32\pi E_a E_b s}\left[C_{\rm const} + C_{\rm lin}W_1 + C_{\rm quad}W_1^2\right], \quad (3.7)$$

where

$$W_1 = m_i^2 + m_c^2 - \frac{1}{2s}(s + m_i^2 - m_j^2)(s + m_c^2 - m_d^2)\,. \quad (3.8)$$

Further, assuming that the incoming particles are non-relativistic implies that $s = (m_i + m_j)^2$. For the most significant annihilation processes, $\tilde{\Pi}_1^+\tilde{\Pi}_1^- \to \tilde{\Pi}_{13}^0\tilde{\Pi}_{13}^0$, $m_c = m_d = 0$ and $m_i^2 \simeq$

$m_j^2 \simeq 64\pi^3 f m_{\rm DM}$. In this limit, the parametric dependence of the s-wave annihilation cross section is:

$$\langle \sigma_{ij} v \rangle_{\rm s-wave} \propto \text{constant} \times \frac{m_{\rm DM}}{f^3} \,, \tag{3.9}$$

where the overall constant is a combination of various traces and found to be $O(1)$ from numerical analysis.

3.2 Freeze-out

The number density of the dark pions, $n_{\rm DP} = n_{\Pi_1^\pm} + n_{\Pi_2^\pm} + n_{\Pi_3^\pm} + n_{\Pi_4^\pm}$, evolves according the Boltzmann equation [33]:

$$\dot{n}_{\rm DP} + 3H n_{\rm DP} = -\langle \sigma_{\rm eff} v \rangle (n_{\rm DP}^2 - n_{\rm DP,eq}^2) \,, \tag{3.10}$$

where $H = \sqrt{8\pi^3 g_*/90}\, T^2/M_{\rm Pl}$ is the Hubble rate during radiation domination, $n_{\rm DP,eq} = g_* m_1^2 T/(2\pi^2) K_2(m_1/T)$ is the equilibrium number density of the lightest dark pion and m_1 is the mass of the lightest DP freezing out, more specifically the mass of $\tilde{\Pi}_1^\pm$. The effective co-annihilation cross-section is defined as

$$\begin{aligned} \sigma_{\rm eff} &= \sum_{i,j=1}^{4} \sigma_{ij} \frac{g_i g_j}{g_{\rm eff}^2} (1+\Delta_i)^{3/2} (1+\Delta_j)^{3/2} e^{-x(\Delta_i+\Delta_j)} \,, \\ \text{with} \quad g_{\rm eff} &= \sum_{i=1}^{4} g_i (1+\Delta_i)^{3/2} e^{-x\Delta_i} \,, \end{aligned} \tag{3.11}$$

where $x = m_1/T$, σ_{ij} is the cross section for the reaction $\tilde{\Pi}_i^\pm \tilde{\Pi}_j^\mp \to \tilde{\Pi}^0 \tilde{\Pi}^0$ given in Eq. (3.7) (summed over all kinematically accessible SM pions in the final state), $g_i = 2$ is the number of degrees of freedom of $\tilde{\Pi}_i^\pm$, and $\Delta_i \equiv (m_i - m_1)/m_1$ is the mass difference between the heavier dark pions and $\tilde{\Pi}_1^\pm$.

In Fig. 4 we present $\langle \sigma_{\rm eff} v \rangle$ for a range of f and $m_{\rm DM}$. By fitting our numerical results to the approximation given in Eq. (3.9), we find the velocity-averaged effective cross-section to be

$$\langle \sigma_{\rm eff} v \rangle \simeq (1.5 - 2) \times 10^{-11}\, \text{GeV}^{-2} \left(\frac{m_{\rm DM}}{5\ \text{TeV}}\right) \left(\frac{65\ \text{TeV}}{f}\right)^3 \,, \tag{3.12}$$

where the lower and higher values correspond to one or three generations of SM fermions respectively. For smaller f and larger constituent DM mass, $\langle \sigma_{\rm eff} v \rangle$ is larger, resulting in too much annihilation and hence not enough dark pions left over to produce the observed abundance of the dark matter. Conversely, a lighter constituent dark matter mass and higher confinement scale result in a lower dark pion annihilation cross-section and an overabundance of dark matter.

3.3 Deconfinement

The freeze-out of the dark pions determines the final comoving number density of dark pions, which has an associated energy density, $\rho_{\rm DP} = m_1 n_{\rm DP}$. At the time of deconfinement, each dark pion flies apart into one χ as well as SM radiation. At that point, the dark matter consists of freely streaming χ particles, with energy density,

$$\rho_{\rm DM} = \frac{m_{\rm DM}}{m_1} \times \rho_{\rm DP} = m_{\rm DM} \times n_{\rm DP} \ , \tag{3.13}$$

which is to be compared with the observed abundance of dark matter from cosmological measurements, $\Omega h^2 = 0.1200 \pm 0.0012$ [35].

We assume that the weak sector deconfines at temperature $T_{\rm dc}$, where $T_{\rm dc} \sim m_1/100$. In estimating the relic density of χ, we assume that the entropy dump into the thermal plasma from the deconfinement process is negligible[1]. After deconfinement, the free χ particles could begin to annihilate into SM through the now unbound weak interactions, for which the cross-section is parametrically $\sigma_{\rm W} \approx \alpha_{\rm W}^2 \pi / m_{\rm DM}^2$, where $\alpha_{\rm W} \sim 0.1$ has presumably returned to the value measured by experiments today. In our numerical scans, we verify that $\sigma_{\rm W}\ n_{\rm DP} \ll H$ at $x = 100$ for the regions of $(m_{\rm DM}, f)$ of interest, ensuring that no period of thermalization after deconfinement occurs and therefore alters the dark matter relic density from Eq. (3.13).

3.4 Numerical Results

We numerically solve Eq. (3.10), adapting the infrastructure of ULYSSES [36], a publicly available PYTHON package developed to solve Boltzmann equations associated with leptogenesis. For each benchmark point, we determine the regions of the parameter space, $(m_{\rm DM}, f)$ that are consistent with the measured relic abundance. To perform this task, we use ULYSSES in conjunction with MULTINEST [37–39] (more precisely, PYMULTINEST [40], a wrapper around MULTINEST written in PYTHON). We place flat priors on the parameters $(m_{\rm DM}, f)$ and employ the log-likelihood as the MULTINEST objective function:

$$\log L = -\frac{1}{2}\left(\frac{\Omega \mathrm{h}^2(m_{\rm DM}, f) - \Omega \mathrm{h}^2_{\rm PDG}}{\Delta \Omega \mathrm{h}^2}\right)^2 \ , \tag{3.14}$$

where $\Omega \mathrm{h}^2(m_{\rm DM}, f)$ is the calculated relic density for a point in the model parameter space, $\Omega \mathrm{h}^2_{\rm PDG}$ is the best-fit value of the relic density and $\Delta \Omega \mathrm{h}^2$ is the 1-σ experimental uncertainty range of the relic abundance [35]. In the left panel of Fig. 4, we show the regions for which the predicted relic abundance of dark matter is consistent with the observed abundance at the one and two sigma. We find that multi-TeV χ masses (and $f \sim 60$ TeV) are favored and consistent with the perturbative unitarity bound [41], which, using the approximate analytic form of $\langle \sigma_{\rm eff} v \rangle$ Eq. (3.9), takes the form:

$$\langle \sigma_{\rm eff} v \rangle_{\rm s-wave} \approx \frac{0.8 m_{\rm DM}}{f^3} \lesssim \frac{4\pi}{64\pi^3 f m_{\rm DM} v} \Rightarrow m_{\rm DM}^2 \lesssim \frac{5 f^2}{64\pi^2 v} \, , \tag{3.15}$$

[1] The vacuum energy in the confined phase is $\sim c_0 \Lambda_W^4$, where c_0 is a constant. We require that this energy is always smaller than the contribution from relativistic degrees of freedom in the Universe, $g_* T^4$. Assuming deconfinement happens at a temperature $T_{\rm dc} = 10^{-4} \Lambda_W$, requiring $c_0 \Lambda_W^4 < g_* T_{\rm dc}^4$ would imply that $c_0 \lesssim 10^{-14}$.

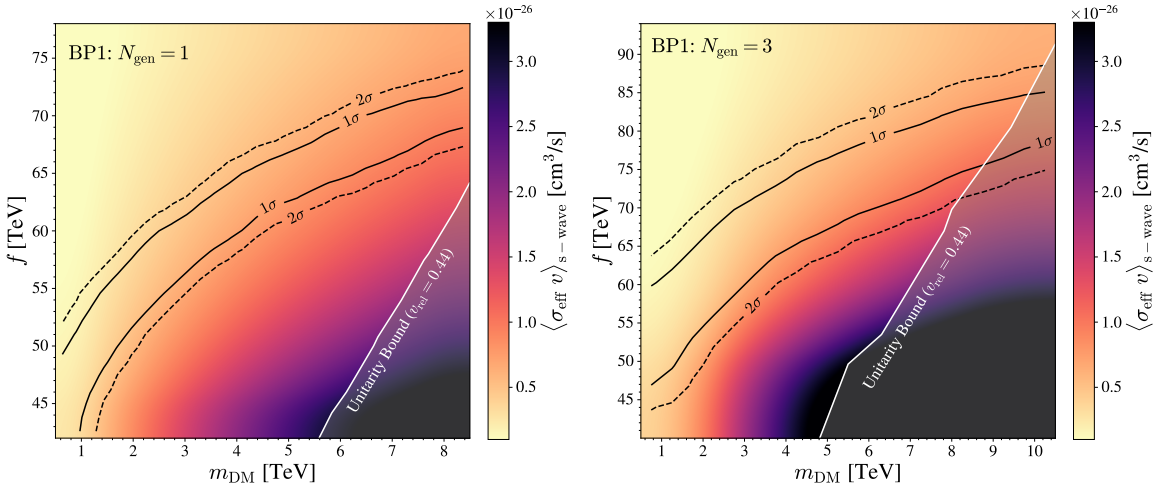

Figure 4: The region of interest for the constituent dark matter mass, $m_{\rm DM}$, and the weak confinement scale, f, for one generation (left) and three generation (right) cases. The solid and dashed lines show where the DM relic density is consistent with observations at 1 and 2 σ respectively. We show the velocity-averaged effective cross section during freeze-out given in Eq. (3.11). The grey shaded area is inconsistent with unitarity constraints. Note that for both cases we start our scan at $m_{\rm DM} = 500$ GeV and that the highest points for our scans are $m_{\rm DM} = 8.5$ TeV and 10.5 TeV for one generation and three generation case respectively. For the benchmark shown above, BP1, $g_s = 0.8, e_Q = 0.5$ and $s_Q^2 = 0.12$.

where we substitute $m_{\rm DP}^2 = 64\pi^3 f m_{\rm DM}$. For a freeze-out temperature of $T_{\rm fo} \simeq m_1/30$, the unitarity limit constrains $m_{\rm DM} \lesssim 1.3f$, which cuts into the parameter regime favored by the relic density at around $m_{\rm DM} \sim 10$ TeV. Fig. 4 shows the unitarity limit on the region of interest using the numerical results for $\langle \sigma_{\rm eff} v \rangle_{\rm s-wave}$. The numerical results for BP1 and BP2 are qualitatively very similar. Our code, which calculates the effective cross-section and solves the Boltzmann equations, for both the one- and three-generation case, is publicly available at .

4 Three Generations of Standard Model doublets and Dark Matter

For simplicity, we have outlined the freeze-out dynamics in the case of a single generation of SM doublets together with the pair of vector-like fermionic SU(2)$_{\rm L}$ doublets ($\{\ell, q^r, q^g, q^b, \chi_1, \chi_2\}$). In this Section, we generalize to three generations ($\{\ell_i, q_i^r, q_i^g, q_i^b, \chi_1, \chi_2\}$ with $i = 1, 2, 3$) where there are 90 pseudo-Goldstone bosons and an η'. The mass matrix is 91×91 and, due to the added complexity of three generations of SM doublets, the mass^2 matrix contains off-diagonal entries which depend non-trivially on the scan parameters $(m_{\rm DM}, f)$. Therefore, unlike in the one generation case, where we could perform the diagonalization of the mass squared matrix analytically, in the three-generation case, we instead rely on a numerical diagonalization of the mass-squared matrix to transform from the interaction to the mass basis for each parameter

Pion (mass basis)	#	Mass squared value	$\mathrm{U}(1)_\mathrm{Q}$ charge	$SU(2)_C$ charge
$\Pi_1^{\rm mass}$	1	$64\pi^2 f\left(7f\kappa+\pi m_{\rm DM}+\sqrt{49f^2\kappa^2-10\pi f\kappa m_{\rm DM}+\pi^2 m_{\rm DM}^2}\right)$	0	1
$\Pi_2^{\rm mass}$	24	$-\frac{1}{2}C_A e_Q^2 f^2-\frac{3}{2}C_G f^2 g_s^2+C_W f^2 g_s^2-\frac{1}{2}C_Z e_Q^2 f^2 s_Q^2+\frac{C_Z e_Q^2 f^2}{6s_Q^2}+\frac{1}{3}C_Z e_Q^2 f^2$	±1	2
$\Pi_3^{\rm mass}$	14	0	0	1
$\Pi_4^{\rm mass}$	6	$-2C_A e_Q^2 f^2-2C_Z e_Q^2 f^2 s_Q^2-\frac{2C_Z e_Q^2 f^2}{9s_Q^2}+\frac{4}{3}C_Z e_Q^2 f^2$	±1	1
$\Pi_5^{\rm mass}$	12	$-\frac{1}{2}C_A e_Q^2 f^2-\frac{3}{2}C_G f^2 g_s^2-C_W f^2 g_s^2-\frac{1}{2}C_Z e_Q^2 f^2 s_Q^2+\frac{C_Z e_Q^2 f^2}{6s_Q^2}+\frac{1}{3}C_Z e_Q^2 f^2$	±1	2
$\Pi_6^{\rm mass}$	6	$64\pi^3 f m_{\rm DM}$	0	1
$\Pi_7^{\rm mass}$	6	$-2C_A e_Q^2 f^2-2C_Z e_Q^2 f^2 s_Q^2+\frac{2}{3}C_Z e_Q^2 f^2+64\pi^3 f m_{\rm DM}$	±1	1
$\Pi_8^{\rm mass}$	9	$-4C_G f^2 g_s^2$	0	3
$\Pi_9^{\rm mass}$	12	$-\frac{1}{2}C_A e_Q^2 f^2-\frac{3}{2}C_G f^2 g_s^2-\frac{1}{2}C_Z e_Q^2 f^2 s_Q^2+\frac{C_Z e_Q^2 f^2}{18s_Q^2}+64\pi^3 f m_{\rm DM}$	±1	2
$\Pi_{10}^{\rm mass}$	1	$64\pi^2 f\left(7f\kappa+\pi m_{\rm DM}-\sqrt{49f^2\kappa^2-10\pi f\kappa m_{\rm DM}+\pi^2 m_{\rm DM}^2}\right)$	0	1

Table 2: Table of mass squared values corresponding to mass basis states along with the relevant $SU(2)_C \times \mathrm{U}(1)_\mathrm{Q}$ charges. Three SM generations with χ_1 and χ_2 are included.

scan point. We perform the same procedure outlined in Section 2.1 to transform from the mass to the $\mathrm{U}(1)_\chi$ basis, and compute annihilation cross-section as described in Section 3.1, but in the three-generation case, there are 12 charged dark pion states. We find that there are ten distinct pion masses as shown in Table. 2. Rather than provide the complete indexing of states, we provide the number of pions (second column) with each mass eigenvalue. Interestingly, several new states, such as the color triplet, appear in the multi-generational case.

In the right panel of Fig. 4, we show the regions for which the predicted relic abundance of dark matter in the three generation case is consistent with the observed abundance. The favored region that explains the DM abundance in the three-generation case is approximately the same as the simplified one generation case but favors slightly higher f values for a given $m_{\rm DM}$. Another slight difference is that the unitarity constraint is more stringent due to the higher values of $\langle\sigma_{\rm eff} v\rangle_{\rm s-wave}$ in the three-generation case.

5 Outlook

Our results indicate that a modification to the strength of the $\mathrm{SU}(2)_\mathrm{L}$ weak coupling dramatically transforms the nature of the freeze-out process for an $\mathrm{SU}(2)_\mathrm{L}$-charged WIMP. For a vector-like pair of doublets, we find that the weak confinement scenario favors a range of masses (depending on the early $\mathrm{SU}(2)_\mathrm{L}$ confinement scale) around $O(1-10)$ TeV and can be much larger than the $\simeq 1.1$ TeV favored by a standard cosmological history [2]. This highlights the possibility that the physics of the dark matter itself could be drastically different at the time of freeze-out from today. In particular, the constraints on a several TeV WIMP are quite different from those restricting a ~ 1 TeV mass particle.

Direct searches for WIMPs scattering with heavy nuclei remain an important challenge. At ~ 10 TeV, XENON1T data restricts the cross-section to scatter with a nucleon to be smaller than about $\sim 10^{-44}$ cm^2 [5], which is still incompatible with the cross-section mediated by full strength Z boson exchange ($\sim 10^{-38}$ cm^2). However, this bound can be avoided by introducing Majorana masses via a dimension-5 operator of the form,

$$\mathcal{L}_{\Delta M} = \frac{1}{M_1}(H^\dagger \chi_1)(H^\dagger \chi_1) + \frac{1}{M_2}(H\chi_2)(H\chi_2) + \text{h.c.} \tag{5.1}$$

where $M_{1,2}$ parameterize the interaction strength and parentheses indicate how $\mathrm{SU}(2)_\mathrm{L}$ indices are contracted. After electroweak breaking, these operators result in Majorana masses of order $v^2/M_{1,2}$, which split the Dirac χ into two Majorana fermions, in close analogy with the see-saw mechanism for generating neutrino masses. The Majorana particles have vanishing vector currents, and thus Z boson exchange mediates inelastic scattering, which is kinematically suppressed once the mass splitting is larger than the typical kinetic energy of the WIMPs in the Galactic halo [42, 43]. Provided the scales M_1 and M_2 are sufficiently large, these operators play essentially no role in freeze-out, and do not themselves mediate an observable scattering with nuclei via Higgs boson exchange.

Despite its full-strength electroweak interactions, a multi-TeV dark matter particle is too heavy to be accessible at the LHC. Even when kinematically accessible, unless there is mixing with another nearby state via electroweak symmetry-breaking, the signatures at colliders are challenging because the charged state is expected to be degenerate with its neutral counterpart to within a few hundred MeV [44], and thus requires mono-jet or disappearing track analyses. As a result, even a future 100 TeV hadron collider is expected to struggle to reach sensitivity to TeV mass electroweak doublets [45].

Indirect searches for the annihilation products of WIMP annihilation, for example, from observation of high energy γ-rays, can reach sensitivity to around 10 TeV for electroweak-sized annihilation cross-sections [6], particularly for masses for which the annihilation experiences a Sommerfeld-like enhancement due to the exchange of weak bosons. These bounds exhibit a considerable sensitivity to the distribution profile of the dark matter around the Galactic center, which is not well constrained by observation (see, e.g. Ref. [7] for discussion). Despite these challenges, a future gamma-ray observatory such as the Cherenkov Telescope Array [46] could offer the best chance of a direct observation of dark matter in such a scenario.

Looking forward, it would be interesting to explore further the consequences of a period of early $\mathrm{SU}(2)_\mathrm{L}$ confinement. It may be that such an epoch could enable new possibilities to understand other mysteries of the early Universe, such as the primordial asymmetry between baryons and anti-baryons. And more widely, our results illustrate the general truth that the early Universe may well turn out to have been more weird and wonderful than simply extrapolating the SM to high temperatures would lead us to expect. Exploring the space of possibilities and how to constrain them with experimental measurements will remain an essential task for particle physics.

Acknowledgements

We are grateful to Holger Schulz for his insightful advice regarding speeding up our Boltzmann code and to Daniel Whiteson for his insight into LHC collider constraints. We thank Joshua Berger and Andrew Long for their helpful comments on the draft. This work was supported in part by the National Science Foundation via grant numbers PHY-1915005 and DGE-1839285. Any opinions, findings and conclusions or recommendations expressed in this material are those of the author(s) and do not necessarily reflect the views of the National Science Foundation. This work used the DiRAC@Durham facility managed by the Institute for Computational Cosmology on behalf of the STFC DiRAC HPC Facility (www.dirac.ac.uk). The equipment was funded by BEIS capital funding via STFC capital grants ST/P002293/1, ST/R002371/1 and ST/S002502/1, Durham University and STFC operations grant ST/R000832/1. DiRAC is part of the National e-Infrastructure.

A Matrices for One Generation

The explicit form of the matrices in Eq. (2.3) for a single generation of Standard Model doublets in addition to χ_1 and χ_2 are:

$$L_1 = \begin{pmatrix} 0&0&0&0&0&0\\ 0&0&0&0&0&0\\ 0&0&0&\frac{1}{2}&0&0\\ 0&0&\frac{1}{2}&0&0&0\\ 0&0&0&0&0&0\\ 0&0&0&0&0&0 \end{pmatrix}, \qquad L_2 = \begin{pmatrix} 0&0&0&0&0&0\\ 0&0&0&0&0&0\\ 0&0&0&-\frac{i}{2}&0&0\\ 0&0&\frac{i}{2}&0&0&0\\ 0&0&0&0&0&0\\ 0&0&0&0&0&0 \end{pmatrix}, \qquad L_3 = \begin{pmatrix} 0&0&0&0&0&0\\ 0&0&0&0&0&0\\ 0&0&\frac{1}{2}&0&0&0\\ 0&0&0&-\frac{1}{2}&0&0\\ 0&0&0&0&0&0\\ 0&0&0&0&0&0 \end{pmatrix},$$

$$Q = \begin{pmatrix} \frac{1}{2}&0&0&0&0&0\\ 0&-\frac{1}{2}&0&0&0&0\\ 0&0&0&0&0&0\\ 0&0&0&0&0&0\\ 0&0&0&0&\frac{1}{2}&0\\ 0&0&0&0&0&-\frac{1}{2} \end{pmatrix}, \qquad L^{1,+} = \begin{pmatrix} 0&0&0&0&0&0\\ 0&0&1&0&0&0\\ 0&0&0&0&0&0\\ 0&0&0&0&0&0\\ 0&0&0&0&0&0\\ 0&0&0&0&0&0 \end{pmatrix}, \qquad L^{2,+} = \begin{pmatrix} 0&0&0&0&0&0\\ 0&0&0&1&0&0\\ 0&0&0&0&0&0\\ 0&0&0&0&0&0\\ 0&0&0&0&0&0\\ 0&0&0&0&0&0 \end{pmatrix},$$

$$L^{1,-} = \begin{pmatrix} 0&0&0&0&0&0\\ 0&0&0&0&0&0\\ 0&1&0&0&0&0\\ 0&0&0&0&0&0\\ 0&0&0&0&0&0\\ 0&0&0&0&0&0 \end{pmatrix}, \qquad L^{2,-} = \begin{pmatrix} 0&0&0&0&0&0\\ 0&0&0&0&0&0\\ 0&0&0&0&0&0\\ 0&1&0&0&0&0\\ 0&0&0&0&0&0\\ 0&0&0&0&0&0 \end{pmatrix}, \qquad M = \frac{m_{\rm DM}}{2} \begin{pmatrix} 0&0&0&0&0&0\\ 0&0&0&0&0&0\\ 0&0&0&0&0&0\\ 0&0&0&0&0&0\\ 0&0&0&0&0&1\\ 0&0&0&0&-1&0 \end{pmatrix},$$

$$J = \begin{pmatrix} -\frac{s_Q^2}{2}&0&0&0&0&0\\ 0&\frac{s_Q^2}{2}-\frac{1}{3}&0&0&0&0\\ 0&0&\frac{1}{6}&0&0&0\\ 0&0&0&\frac{1}{6}&0&0\\ 0&0&0&0&-\frac{s_Q^2}{2}&0\\ 0&0&0&0&0&\frac{s_Q^2}{2} \end{pmatrix}. \tag{A.1}$$

References

[1] G. Bertone and T. Tait, M. P., *A new era in the search for dark matter*, *Nature* **562** (2018) 51–56, [1810.01668].

[2] M. Cirelli, N. Fornengo and A. Strumia, *Minimal dark matter*, *Nucl. Phys. B* **753** (2006) 178–194, [hep-ph/0512090].

[3] ATLAS collaboration, G. Aad et al., *Search for new phenomena in events with an energetic jet and missing transverse momentum in pp collisions at $\sqrt{s}$ =13 TeV with the ATLAS detector*, *Phys. Rev. D* **103** (2021) 112006, [2102.10874].

[4] CMS collaboration, *Search for new particles in events with energetic jets and large missing transverse momentum in proton-proton collisions at* $\sqrt{s} = 13$ TeV, .

[5] XENON collaboration, E. Aprile et al., *Dark Matter Search Results from a One Ton-Year Exposure of XENON1T*, *Phys. Rev. Lett.* **121** (2018) 111302, [1805.12562].

[6] MAGIC, Fermi-LAT collaboration, M. L. Ahnen et al., *Limits to Dark Matter Annihilation Cross-Section from a Combined Analysis of MAGIC and Fermi-LAT Observations of Dwarf Satellite Galaxies*, *JCAP* **02** (2016) 039, [1601.06590].

[7] J. Arakawa and T. M. P. Tait, *Is a Miracle-less WIMP Ruled Out?*, 2101.11031.

[8] S. Hamdan and J. Unwin, *Dark Matter Freeze-out During Matter Domination*, *Mod. Phys. Lett. A* **33** (2018) 1850181, [1710.03758].

[9] G. B. Gelmini and P. Gondolo, *Neutralino with the right cold dark matter abundance in (almost) any supersymmetric model*, *Phys. Rev. D* **74** (2006) 023510, [hep-ph/0602230].

[10] D. Berger, S. Ipek, T. M. P. Tait and M. Waterbury, *Dark Matter Freeze Out during an Early Cosmological Period of QCD Confinement*, *JHEP* **07** (2020) 192, [2004.06727].

[11] L. Heurtier, F. Huang and T. M. P. Tait, *Resurrecting Low-Mass Axion Dark Matter Via a Dynamical QCD Scale*, 2104.13390.

[12] J. Berger, A. J. Long and J. Turner, *Phase of confined electroweak force in the early Universe*, *Phys. Rev. D* **100** (2019) 055005, [1906.05157].

[13] L. F. Abbott and E. Farhi, *Are the Weak Interactions Strong?*, *Phys. Lett.* **101B** (1981) 69–72.

[14] L. F. Abbott and E. Farhi, *A Confining Model of the Weak Interactions*, *Nucl. Phys. B* **189** (1981) 547–556.

[15] M. Claudson, E. Farhi and R. L. Jaffe, *The Strongly Coupled Standard Model*, *Phys. Rev.* **D34** (1986) 873.

[16] G. 't Hooft, *Topological aspects of quantum chromodynamics*, in *From the Planck length to the Hubble radius. Proceedings, International School of Subnuclear Physics, Erice, Italy, August 29-September 7, 1998*, pp. 216–236, 1998. hep-th/9812204.

[17] X. Calmet and H. Fritzsch, *The Electroweak interaction as a confinement phenomenon*, *Phys. Lett.* **B496** (2000) 161–168, [hep-ph/0008243].

[18] X. Calmet and H. Fritzsch, *Calculation of the Higgs boson mass using the complementarity principle*, *Phys. Lett. B* **525** (2002) 297–300, [hep-ph/0107085].

[19] X. Calmet and H. Fritzsch, *Electroweak D waves*, *Phys. Lett. B* **526** (2002) 90–96, [hep-ph/0103333].

[20] N. Lohitsiri and D. Tong, *If the Weak Were Strong and the Strong Were Weak*, *SciPost Phys.* **7** (2019) 059, [1907.08221].

[21] J. Preskill, *Subgroup Alignment in Hypercolor Theories*, *Nucl. Phys. B* **177** (1981) 21–59.

[22] D. A. Kosower, *SYMMETRY BREAKING PATTERNS IN PSEUDOREAL AND REAL GAUGE THEORIES*, *Phys. Lett. B* **144** (1984) 215–216.

[23] R. Lewis, C. Pica and F. Sannino, *Light Asymmetric Dark Matter on the Lattice: SU(2) Technicolor with Two Fundamental Flavors*, *Phys. Rev. D* **85** (2012) 014504, [1109.3513].

[24] R. Arthur, V. Drach, M. Hansen, A. Hietanen, C. Pica and F. Sannino, *SU(2) gauge theory with two fundamental flavors: A minimal template for model building*, *Phys. Rev. D* **94** (2016) 094507, [1602.06559].

[25] T. Karavirta, J. Rantaharju, K. Rummukainen and K. Tuominen, *Determining the conformal window: SU(2) gauge theory with N_f = 4, 6 and 10 fermion flavours*, *JHEP* **05** (2012) 003, [1111.4104].

[26] M. Hayakawa, K. I. Ishikawa, S. Takeda, M. Tomii and N. Yamada, *Lattice Study on quantum-mechanical dynamics of two-color QCD with six light flavors*, *Phys. Rev. D* **88** (2013) 094506, [1307.6696].

[27] A. Amato, T. Rantalaiho, K. Rummukainen, K. Tuominen and S. Tähtinen, *Approaching the conformal window: systematic study of the particle spectrum in SU(2) field theory with N_f =2,4 and 6.*, *PoS* **LATTICE2015** (2016) 225, [1511.04947].

[28] V. Leino, K. Rummukainen, J. M. Suorsa, K. Tuominen and S. Tähtinen, *Infrared fixed point of SU(2) gauge theory with six flavors*, *Phys. Rev. D* **97** (2018) 114501, [1707.04722].

[29] V. Leino, K. Rummukainen and K. Tuominen, *Slope of the beta function at the fixed point of SU(2) gauge theory with six or eight flavors*, *Phys. Rev. D* **98** (2018) 054503, [1804.02319].

[30] T. Das, G. S. Guralnik, V. S. Mathur, F. E. Low and J. E. Young, *Electromagnetic mass difference of pions*, *Phys. Rev. Lett.* **18** (1967) 759–761.

[31] V. Ayyar, M. F. Golterman, D. C. Hackett, W. Jay, E. T. Neil, Y. Shamir et al., *Radiative Contribution to the Composite-Higgs Potential in a Two-Representation Lattice Model*, *Phys. Rev. D* **99** (2019) 094504, [1903.02535].

[32] A. Manohar and H. Georgi, *Chiral Quarks and the Nonrelativistic Quark Model*, *Nucl. Phys. B* **234** (1984) 189–212.

[33] K. Griest and D. Seckel, *Three exceptions in the calculation of relic abundances*, *Phys. Rev. D* **43** (1991) 3191–3203.

[34] G. Servant and T. M. P. Tait, *Is the lightest Kaluza-Klein particle a viable dark matter candidate?*, *Nucl. Phys. B* **650** (2003) 391–419, [hep-ph/0206071].

[35] Planck collaboration, N. Aghanim et al., *Planck 2018 results. VI. Cosmological parameters*, *Astron. Astrophys.* **641** (2020) A6, [1807.06209].

[36] A. Granelli, K. Moffat, Y. F. Perez-Gonzalez, H. Schulz and J. Turner, *ULYSSES: Universal LeptogeneSiS Equation Solver*, *Comput. Phys. Commun.* **262** (2021) 107813, [2007.09150].

[37] F. Feroz, M. P. Hobson and M. Bridges, *MultiNest: an efficient and robust Bayesian inference tool for cosmology and particle physics*, *Mon. Not. Roy. Astron. Soc.* **398** (2009) 1601–1614, [0809.3437].

[38] F. Feroz and M. P. Hobson, *Multimodal nested sampling: an efficient and robust alternative to MCMC methods for astronomical data analysis*, *Mon. Not. Roy. Astron. Soc.* **384** (2008) 449, [0704.3704].

[39] F. Feroz, M. P. Hobson, E. Cameron and A. N. Pettitt, *Importance Nested Sampling and the MultiNest Algorithm*, *ArXiv e-prints* (June, 2013) , [1306.2144].

[40] Buchner, J., Georgakakis, A., Nandra, K., Hsu, L., Rangel, C., Brightman, M. et al., *X-ray spectral modelling of the agn obscuring region in the cdfs: Bayesian model selection and catalogue*, *A&A* **564** (2014) A125.

[41] K. Griest and M. Kamionkowski, *Unitarity Limits on the Mass and Radius of Dark Matter Particles*, *Phys. Rev. Lett.* **64** (1990) 615.

[42] D. Tucker-Smith and N. Weiner, *Inelastic dark matter*, *Phys. Rev. D* **64** (2001) 043502, [hep-ph/0101138].

[43] J. Bramante, P. J. Fox, G. D. Kribs and A. Martin, *Inelastic frontier: Discovering dark matter at high recoil energy*, *Phys. Rev. D* **94** (2016) 115026, [1608.02662].

[44] R. J. Hill and M. P. Solon, *Universal behavior in the scattering of heavy, weakly interacting dark matter on nuclear targets*, *Phys. Lett. B* **707** (2012) 539–545, [1111.0016].

[45] M. Low and L.-T. Wang, *Neutralino dark matter at 14 TeV and 100 TeV*, *JHEP* **08** (2014) 161, [1404.0682].

[46] CTA collaboration, A. Acharyya et al., *Sensitivity of the Cherenkov Telescope Array to a dark matter signal from the Galactic centre*, *JCAP* **01** (2021) 057, [2007.16129].